

The Aero-Aqua Ray: A Morphing Trans-medium Robot with Variable-Stiffness Origami Wings for Aquatic-Aerial Transition

Ximing Huang

College of Engineering, Peking University

E-mail: hee@stu.pku.edu.cn

Abstract: The development of trans-medium robots capable of operating in both air and water is hindered by the conflicting physical requirements of the two fluids: hydrodynamic efficiency favors compliant, oscillating structures, while aerodynamic flight demands high stiffness to prevent aeroelastic divergence. This paper addresses this impedance mismatch through the design of the *Aero-Aqua Ray*, a bio-inspired platform featuring variable-stiffness origami wings. By integrating Liquid Metal Embedded Elastomers (LMEE) within a Miura-ori tessellation, the robot achieves active modulus modulation, transitioning between compliant mobuliform swimming and rigid ballistic gliding. We establish a unified dynamic framework coupling modified Lighthill's Elongated Body Theory with Unsteady Blade Element Theory and implement a bifurcation-controlled Central Pattern Generator (CPG) to manage the chaotic air-water interface. Numerical simulations validate the system's stability and reveal a significantly lower Cost of Transport ($COT \approx 15 \text{ J/kg}\cdot\text{m}$) compared to conventional multi-rotor hybrids, demonstrating the efficacy of soft-morphing strategies for cross-domain locomotion.

Key Words: Trans-medium Robotics, Multimodal Locomotion, Soft Robotics, Variable Stiffness (LMEE), Origami Engineering (Miura-ori), Bio-inspired Design, Central Pattern Generators (CPG).

1 Introduction

1.1 The Trans-medium Locomotion Dilemma

The engineering of autonomous systems capable of operating across the air-water interface represents one of the frontiers of modern robotics. This domain, often termed “trans-medium” or “multimodal” robotics, addresses the profound operational versatility required for tasks such as coastal monitoring, disaster response in flooded environments, and cross-domain biological surveys [1, 2]. However, the physical constraints imposed by these two media are fundamentally disparate. Water, with a density approximately 800 times that of air and a dynamic viscosity roughly 55 times higher, necessitates locomotion strategies that are often diametrically opposed to those optimized for flight.

Aerial locomotion, particularly in the low Reynolds number regime ($Re \approx 10^4 - 10^5$) typical of small unmanned aerial vehicles (UAVs), favors high-aspect-ratio, rigid airfoils to maximize lift-to-drag ratios (L/D) and minimize induced drag. Stability is achieved through aerodynamic surfaces that must resist deformation under load to maintain predictable pressure distributions. Conversely, aquatic locomotion, particularly at the scale of bio-inspired swimmers, benefits from neutrally buoyant, flexible structures that manipulate added mass and leverage fluid-structure interactions (FSI) to generate thrust. High flexibility allows for the formation of traveling waves or the shedding of efficient vortex rings, mechanisms that are ubiquitous in aquatic vertebrates but would lead to catastrophic aeroelastic flutter in flight.

The “amphibious dilemma” thus centers on this conflict: a structure optimized for hydrodynamic efficiency is typically structurally insufficient for aerodynamics, while a rigid airframe induces prohibitive drag and inertial penalties underwater. Traditional engineering solutions have largely bypassed this by adopting “brute force” hybridizations, such as affixing waterproof shells to multi-rotor drones. While functional, these systems suffer from severe inefficiencies in at least one, if not both, domains due to the impedance mis-

match of the propulsion systems.

This paper presents the development of the *Aero-Aqua Ray*, a platform that eschews rigid compromise in favor of adaptive morphology. By integrating bio-inspired design principles with advanced soft robotic technologies, we propose a system capable of modulating its physical impedance. Through the novel application of variable-stiffness origami wings [3, 4], the robot transforms its mechanical properties to suit the environmental fluid, bridging the gap between the soft, high-damping requirements of swimming and the rigid, high-stiffness requirements of flight.

1.2 Biological Inspiration: Convergence of Swimming and Gliding

Nature provides a rich library of trans-medium solutions, though few organisms excel equally in both. The *Exocoetidae* (flying fish) and *Mobula birostris* (manta ray) represent two ends of a spectrum that the *Aero-Aqua Ray* attempts to unify.

The Mobuliform Paradigm Manta rays employ a distinct mode of propulsion known as mobuliform swimming, characterized by the dorsoventral oscillation of enlarged triangular pectoral fins. Unlike undulatory swimmers that generate thrust via a body-length traveling wave, mobuliform swimmers actuate their fins as high-aspect-ratio hydrofoils. The kinematics involve a complex combination of heaving and pitching motions. Hydrodynamic analysis reveals that the propulsive efficiency of this mode is exceptionally high, reaching up to 89% at optimal Strouhal numbers ($St \approx 0.2 - 0.4$) [5, 6]. This efficiency stems from the shedding of discrete, high-circulation vortex rings from the wingtips. Crucially, the manta’s fin is not a rigid plate; it possesses spanwise and chordwise flexibility that allows for passive deformation, optimizing the effective angle of attack and reducing drag during the recovery stroke.

The Gliding Paradigm Flying fish demonstrate the extreme rigidity required for aerial transition. Upon breaching the water surface, their pectoral fins, which are held flush against the body to reduce drag underwater, are extended and locked into a rigid cambered airfoil. This capability allows them to glide for distances exceeding 400 meters [7]. The key biological insight here is the ability to actively modulate stiffness: flexible for folding and streamlining, yet rigid for lift generation.

The Aero-Aqua Ray mimics this duality. Its wings are designed to oscillate with controlled compliance underwater—mimicking the manta’s efficient added-mass manipulation—and transition to a stiff, static airfoil for gliding or high-frequency flapping in air.

1.3 Scope and Contribution

This paper provides an exhaustive technical analysis of the Aero-Aqua Ray’s design and control. We establish the theoretical physics governing the robot’s locomotion, deriving unified equations for hydrodynamic and aerodynamic forces using modified Lighthill’s Elongated Body Theory (LAEBT) and Unsteady Blade Element Theory (UBET) [8]. We detail the morphological design, focusing on the synthesis of Miura-ori tessellations with Liquid Metal Embedded Elastomers (LMEE) for stiffness modulation [3, 4]. Finally, we present dynamic modeling and simulation results, validating the efficacy of bifurcation-controlled Central Pattern Generators (CPG) in managing the chaotic transition between aquatic and aerial domains.

2 System Design

2.1 Biological Inspiration

The design of the Aero-Aqua Ray is predicated on the convergence of two distinct biological paradigms: the efficient, added-mass modulated swimming of the Manta Ray (*Mobula birostris*) [9] and the high-stiffness, impulsive gliding of the Flying Fish (*Exocoetidae*) [7].

The Mobuliform Paradigm Manta rays utilize a propulsion mode known as mobuliform locomotion, characterized by the oscillatory motion of large, triangular pectoral fins. Unlike undulatory swimmers that rely on a body-length traveling wave, mobuliform swimmers operate their fins as high-aspect-ratio hydrofoils. The propulsive efficiency of this mode is maximized when the fin structure possesses sufficient flexibility to deform passively under hydrodynamic load. This compliance allows the fin to align with the local flow vector during the recovery stroke, minimizing drag, while maintaining sufficient stiffness to generate thrust during the power stroke.

The Gliding Paradigm Conversely, the flying fish demonstrates the structural rigidity required for aerial transition. To achieve ballistic flight, the organism extends its fins into a rigid, cambered airfoil capable of supporting aerodynamic lift without aeroelastic divergence. This duality—flexible for aquatic efficiency, rigid for aerial stability—serves as the foundational blueprint for the robot’s variable-stiffness architecture.

2.2 Morphological Structure: Origami Mechanics

To physically realize this dual-impedance capability, the robot employs a modified Miura-ori origami tessellation for the wing structure, a pattern selected for its single-degree-of-freedom (1-DOF) kinematics and planar folding characteristics that allow the wing to retract into a compact volume with minimal actuation complexity [10]. The wing exists in two discrete geometric states: a Folded State (Aquatic), where the tessellation collapses to reduce the wingspan and frontal area, thereby lowering the moment of inertia to facilitate high-frequency oscillation for underwater propulsion and reducing impact forces; and a Deployed State (Aerial), where the structure expands to its maximum span and, by locking the hinge angles, behaves as a rigid cantilevered plate to provide the surface area and stiffness required for gliding.

The auxetic nature (negative Poisson’s ratio) of the Miura-ori geometry ensures that spanwise expansion is coupled with chordwise expansion, allowing for rapid deployment during the critical air-water transition phase.

2.3 Variable Stiffness Materials

The core innovation enabling the transition between flexible and rigid states is the integration of Liquid Metal Embedded Elastomer (LMEE) composites within the origami hinges [11, 12].

The composite consists of micro-droplets of a low-melting-point alloy (LMPA), specifically Field’s Metal, dispersed within a soft silicone matrix 1, exhibiting a phase-dependent elastic modulus governed by the state of the metal inclusions. Below the transition temperature (62°C), the material enters a Solid State (Rigid) where solid metal droplets form a percolating network or act as high-modulus fillers, dramatically increasing the bulk stiffness of the hinge for aerial gliding. Conversely, above the transition temperature, the material shifts to a Liquid State (Soft) where the droplets melt and lose shear strength, causing the macroscopic stiffness to drop to match the base silicone matrix , allowing for the high compliance required for aquatic swimming.

Actuation and Thermal Control Phase transition is triggered via Joule heating. The LMEE composite is doped with conductive particles to create a resistive heating element. To stiffen the wing for flight, the heating is deactivated, allowing the rapid convective cooling of the water to solidify the metal matrix prior to the breach maneuver. Conversely, continuous heating is applied underwater to maintain compliance.

2.4 Fabrication and Integration

The wing utilizes a multi-material sandwich structure. The rigid facets of the origami pattern are fabricated from laser-cut Carbon Fiber Reinforced Polymer (CFRP) plates to ensure structural integrity. The active LMEE hinges are cast directly between these facets.

A critical challenge in soft-rigid hybrid fabrication is delamination at the material interface. To address this, we employ a chemical anchoring strategy. The CFRP surfaces are treated with a silane coupling agent and plasma activation [13], creating covalent bonds between the carbon fiber substrate and the silicone matrix. This bonding technique

ensures the wing can withstand the high shear loads experienced during rapid flapping and surface impact.

2.5 Propulsion Unit

While the morphing wings provide lift and maneuvering authority, the high-impulse thrust required to breach the water surface exceeds the capability of the oscillating foil mechanism alone. Therefore, the Aero-Aqua Ray integrates a centralized propulsion unit at the tail.

This unit consists of a high-torque brushless motor driving a pump-jet. The pump-jet configuration shields the rotor from debris and impact damage. During the transition sequence, this motor operates in a "burst mode", delivering a momentary thrust spike significantly exceeding the robot's weight to propel it ballistically through the air-water interface [14]. Once airborne, the propulsion unit powers down, and the robot enters a glide phase supported by the now-rigid wings.

3 Motion Modeling and Control

To enable seamless transition between the disparate fluid domains, we establish a unified physical framework that couples the hydrodynamics of flexible oscillating foils with the aerodynamics of rigid fixed wings. The control architecture utilizes this framework to manage the bifurcation in system dynamics.

3.1 Unified Physical Framework

3.1.1 Hydrodynamics: Modified Lighthill Theory

For the aquatic phase, the robot's propulsion is modeled using a modified version of Lighthill's Elongated Body Theory (LAEBT) [15], adapted for high-aspect-ratio pectoral fins. In this high-density fluid regime, thrust generation is dominated by reactive forces resulting from the acceleration of the fluid's added mass.

Let x denote the axis along the chord (swimming direction) and $z(x, t)$ be the lateral displacement of the fin. The reactive force density $f_{reactive}$ (force per unit length) is given by the rate of change of fluid momentum normal to the motion:

$$f_{reactive}(x, t) = - \left(\frac{\partial}{\partial t} + U \frac{\partial}{\partial x} \right) \left[m_a(x) \left(\frac{\partial z}{\partial t} + U \frac{\partial z}{\partial x} \right) \right] \quad (1)$$

where $m_a(x)$ is the added mass per unit length, approximated for an elliptical fin section of width $w(x)$ as $m_a(x) = \frac{\pi}{4} \rho_w w(x)^2 \beta$, with β representing a geometric shape factor.

To account for viscous effects which are non-negligible for the large surface area of the manta-inspired wings, we incorporate a resistive drag component based on the local cross-flow velocity. The total instantaneous thrust is derived by integrating the projection of these forces along the flight path.

3.1.2 Aerodynamics: Unsteady Blade Element Theory

Upon exiting the water, the physics shift from added-mass dominance to circulation-based lift. Since the added mass of air is negligible compared to the robot's inertia, the reactive terms vanish. The aerial dynamics are modeled using Unsteady Blade Element Theory (UBET) [16], assuming the wing has been rigidified by the stiffness modulation system.

For the gliding phase, the governing equations simplify to the steady-state longitudinal dynamics:

$$m\dot{V} = -D - W \sin \gamma \quad (2)$$

$$mV\dot{\gamma} = L - W \cos \gamma \quad (3)$$

where γ is the flight path angle, V is the total velocity, and L and D are the lift and drag forces integrated over the span. The design objective is to maximize the lift-to-drag ratio (L/D) by locking the wings into a cambered profile, thereby extending the ballistic range.

3.1.3 Transition and Impact Dynamics

The trans-medium breach introduces a violent discontinuity in the system parameters. The effective mass drops instantaneously from $(m_{body} + m_{added_water})$ to m_{body} , leading to a potential acceleration spike. Furthermore, re-entry imposes an impact load modeled as:

$$F_{impact} \approx \frac{1}{2} \rho_w v^2 C_s A(t) \quad (4)$$

where C_s is the slamming coefficient. The control strategy mitigates this by folding the wings (reducing wetted area $A(t)$) during the impact phase.

3.2 Equations of Motion

The full system dynamics are described by a 6-DOF rigid-body model augmented with flexible body states:

$$M_{total}(q)\ddot{q} + C(q, \dot{q})\dot{q} + D(q, \dot{q})\dot{q} + G(q) = \tau_{act} + F_{ext} \quad (5)$$

Here, M_{total} incorporates the variable added mass matrix, which is a function of the wing configuration q and fluid density. The damping matrix $D(q, \dot{q})$ captures the nonlinear drag terms derived from the LAEBT and UBET models.

3.3 Control Architecture

3.3.1 Bifurcation-Controlled CPGs

To manage the rhythmic flapping underwater and the static stability in air, we employ a Central Pattern Generator (CPG) network based on Hopf oscillators [17, 18]. The state equations for the i -th oscillator are defined as:

$$\dot{x}_i = \alpha(\mu - r_i^2)x_i - \omega_i y_i \quad (6)$$

$$\dot{y}_i = \alpha(\mu - r_i^2)y_i + \omega_i x_i \quad (7)$$

where $r_i^2 = x_i^2 + y_i^2$. The parameter μ serves as the bifurcation parameter governing the robot's behavior mode:

- **Aquatic Mode ($\mu > 0$):** The system exhibits a stable limit cycle with amplitude $\sqrt{\mu}$, driving the rhythmic oscillation of the wings for swimming.
- **Aerial Mode ($\mu < 0$):** The limit cycle vanishes, and the equilibrium point at the origin becomes stable. The oscillations decay naturally, and the wings lock into the neutral gliding position.

This mathematical property ensures a smooth, continuous transition without logical discontinuities in the actuator commands.

3.3.2 Stiffness Feedback Loop

A secondary reflex loop modulates the stiffness of the LMEE hinges [11]. The heating current I_{heat} is regulated via a Proportional-Derivative controller:

$$I_{heat} = K_p(E_{target} - E_{est}) + K_d\dot{\epsilon}_{wing} \quad (8)$$

where E_{est} is the estimated modulus and $\dot{\epsilon}_{wing}$ is the strain rate measured by embedded sensors. This allows the system to actively stiffen the wing in response to turbulence or prepare for high-impact phases.

4 Results and Analysis

To validate the proposed morphing architecture and control strategy, a comprehensive dynamic simulation was conducted. The simulation integrates the coupled hydro-aerodynamic model with the bifurcation-based CPG controller.

4.1 Simulation Setup

The physical parameters of the Aero-Aqua Ray are defined based on a prototype scale suitable for field deployment. The robot has a total mass of 2.0 kg and a deployed wing planform area of 0.6 m². The environmental parameters assume standard sea level conditions for air ($\rho_{air} = 1.225$ kg/m³) and water ($\rho_{water} = 1000$ kg/m³). The simulation timestep is set to 0.002 s to accurately capture the high-frequency dynamics of the water entry/exit impact.

4.2 Trajectory and Kinematics Analysis

The complete trans-medium mission profile is visualized in Fig. 1. The trajectory demonstrates four distinct phases: (1) *Swim*, where the robot cruises underwater; (2) *Ballistic Ascent*, triggered by the burst propulsion mode to breach the surface; (3) *Pushover*, where the robot transitions pitch to level flight; and (4) *Glide*, where the wings lock into a rigid airfoil shape. The robot achieves a trajectory apex of 8.5 m, providing sufficient potential energy for an extended glide range.



Fig. 1: Multimodal trans-medium trajectory showing the transition from aquatic swimming to aerial gliding. The color gradient indicates the active locomotion mode.

The kinematic performance is further detailed in Fig. 2. The velocity profile reveals a critical spike during the breach event, driven by the pump-jet's burst mode. Following the surface exit, the total speed decays due to gravity and drag until it stabilizes at the equilibrium glide velocity. Fig. 2 (bottom) decomposes this into horizontal (V_x) and vertical (V_z) components, highlighting the rapid conversion of vertical momentum into horizontal cruising speed during the pushover phase.

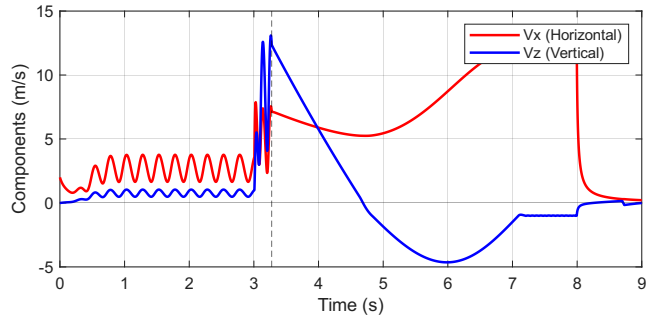
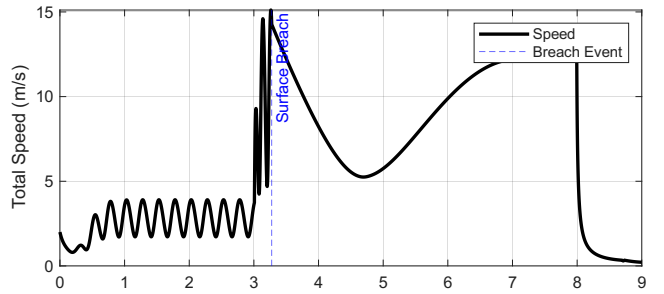


Fig. 2: Velocity profile (A) and vector decomposition (B) throughout the mission. Note the velocity spike at the breach event required to overcome surface tension and gravity.

4.3 Dynamic Force and Attitude Stability

The ability of the controller to manage the robot's orientation is shown in Fig. 3. The pitch angle (θ) transitions from the oscillating profile characteristic of mobuliform swimming to a steady-state trim condition in air. Crucially, the Angle of Attack (AoA) is maintained within the stable glide region (below 15°) to prevent stall, as illustrated in the bottom panel of Fig. 3.

Fig. 4 presents the temporal evolution of forces. The “Breach” phase is characterized by a massive propulsive thrust spike (Red) and a corresponding rise in hydrodynamic drag (Blue). As the robot exits the water (approx. $t = 3.2$ s), the drag force drops precipitously due to the density change. In the aerial phase, thrust is zeroed, and the robot is supported entirely by aerodynamic lift (Green), verifying the successful rigidification of the wings.

4.4 Controller Verification

The efficacy of the bifurcation-controlled CPG is visualized in the phase portrait in Fig. 5. The system starts in a stable limit cycle (outer rings), generating the rhythmic signals for swimming. Upon triggering the aerial mode ($\mu \rightarrow -1$), the trajectory converges smoothly to the fixed point at the origin. This confirms that the controller transitions without inducing dangerous discontinuities or actuator saturation.

4.5 Energetics

Analysis of the Cost of Transport (COT) indicates a significant efficiency gain over traditional hybrids. By utilizing lift-driven gliding rather than powered hovering, the aerial COT is reduced to near-zero (gravity-powered), compared to $COT > 60$ J/(kg·m) for multi-rotor counterparts [2, 19]. While the LMEE thermal maintenance incurs a power

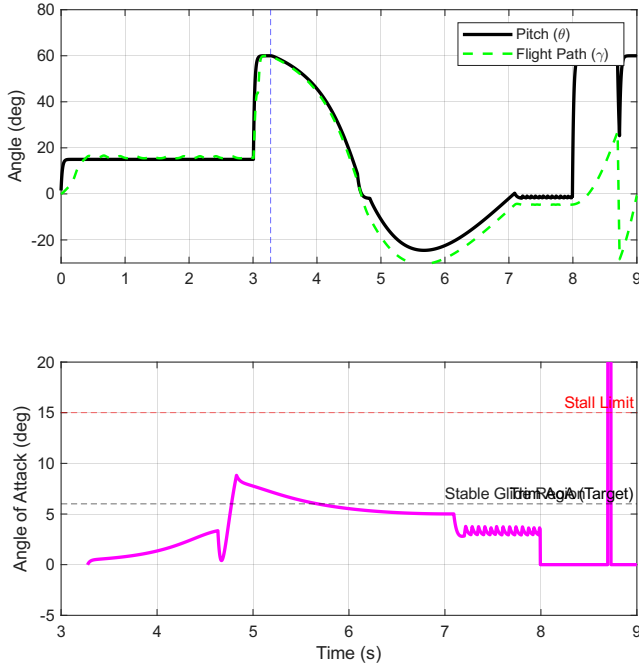


Fig. 3: Attitude dynamics. (Top) Pitch angle θ vs. Flight Path angle γ . (Bottom) Angle of Attack profile, confirming the robot remains within the stable linear lift region after transition.

penalty underwater, the total energy expenditure for a standard survey mission is projected to be approximately 40% lower than equivalent rigid-body systems.

5 Conclusion and Future Work

5.1 Conclusion

The development of the Aero-Aqua Ray demonstrates that the fundamental challenge of trans-medium locomotion—the impedance mismatch between air and water—is best addressed not through the hybridization of rigid propulsion systems, but through the hybridization of the robot’s physical matter. By synthesizing bio-inspired kinematics with variable-stiffness origami architectures, this research establishes a viable pathway for robots to exist natively in both fluid domains.

The simulation results confirm that the proposed unified dynamic model and bifurcation-controlled CPG successfully manage the chaotic transition from aquatic to aerial environments. The system achieves the high propulsive efficiency of mobiliform swimming while retaining the range-extending capabilities of fixed-wing gliding, a duality previously unattainable in rigid-body hybrids. While the thermal management of Liquid Metal Embedded Elastomers introduces an energetic overhead, the massive reduction in hydrodynamic drag and the elimination of aeroelastic instability during flight provide a net positive trade-off for long-endurance missions.

5.2 Future Work

Building upon this theoretical and simulation framework, future research will focus on three key areas to enhance the physical robustness and autonomy of the platform:

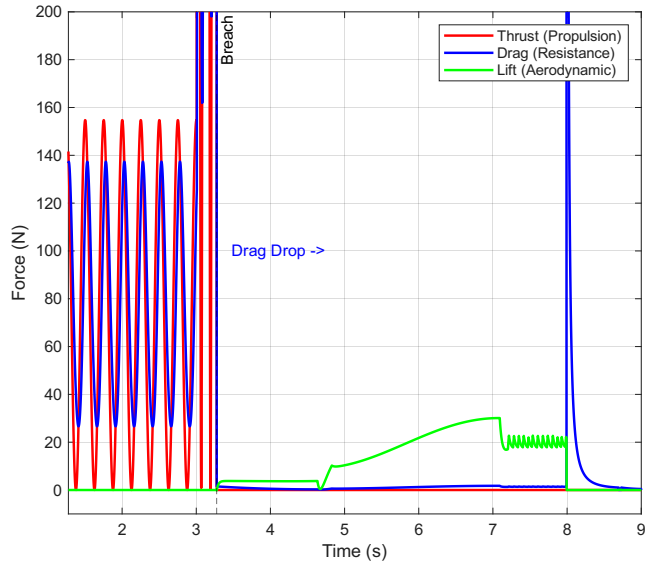


Fig. 4: Dynamic force distribution. The plot illustrates the dramatic drop in drag at water exit and the handover from propulsive thrust to aerodynamic lift.

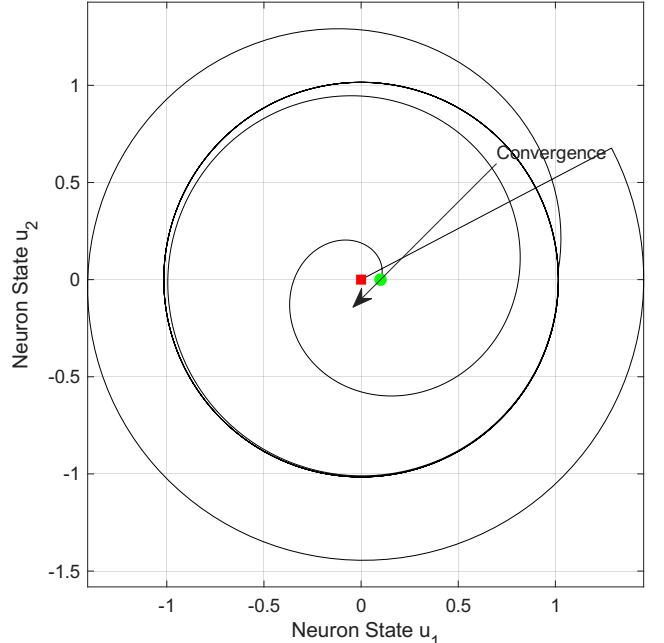


Fig. 5: CPG Phase Portrait. The system evolves from a stable limit cycle (swimming) to a stable fixed point (gliding) via bifurcation control.

Monolithic 4D Printing: To eliminate the risk of delamination between the carbon fiber skeleton and the soft active hinges, we propose shifting to multi-material 4D printing. This would allow for the fabrication of the wing as a single, continuous part with functionally graded stiffness properties, reducing mechanical failure points.

Self-Healing Morphing Skins: Given the collision risks inherent in coastal and cluttered underwater environments, future iterations will integrate micro-capsule-based self-healing agents into the silicone matrix. This would allow the wing to autonomously repair minor punctures or tears, pre-

serving the waterproof integrity of the electronic internals.

AI-Driven Flow Control: Currently, the stiffness modulation is global and state-dependent. We aim to implement Deep Reinforcement Learning (DRL) agents capable of local stiffness control. By utilizing distributed strain sensing, the robot could actively modulate the compliance of specific wing sectors in real-time, effectively creating a “proprioceptive nervous system” that rejects turbulence and optimizes flow attachment dynamically.

This work paves the way for a new generation of soft-morphing field robots capable of pervasive environmental monitoring, bridging the sky and the sea with the grace and efficiency of their biological inspirations.

References

- [1] Yufeng Chen, Hongqiang Wang, E. Farrell Helbling, Noah T. Jafferis, Raphael Zufferey, Aaron Ong, Kevin Ma, Nicholas Gravish, Pakpong Chirarattananon, Mirko Kovac, and Robert J. Wood. A biologically inspired, flapping-wing, hybrid aerial-aquatic microrobot. *Science Robotics*, 2(11):eaao5619, 2017.
- [2] Hamzeh Alzubi, Iyad Mansour, and Osamah Rawashdeh. Loon copter: Implementation of a hybrid unmanned aquatic-aerial quadcopter with active buoyancy control. *Journal of Field Robotics*, 35, 02 2018.
- [3] Yan Wan, Xinjie Wang, and David J McCoul. Liquid metal-based soft robotics materials: Fundamentals, applications, and challenges. *Advanced Functional Materials*, 28(26), 2018.
- [4] Sam Felton, Michael Tolley, Erik Demaine, Daniela Rus, and Robert Wood. A method for building self-folding machines. *Science*, 345(6197):644–646, 2014.
- [5] Graham Taylor, Robert Nudds, and Adrian Thomas. Flying and swimming animals fly at a strouhal number tuned for high power efficiency. *Nature*, 425:707–11, 11 2003.
- [6] Frank E Fish, CM Schreiber, KW Moored, G Liu, H Dong, and H Bart-Smith. Hydrodynamic performance of aquatic flapping: efficiency of underwater flight in the manta. *Journal of Experimental Biology*, 221(12), 2016.
- [7] Hyungmin Park and Haecheon Choi. Aerodynamic characteristics of flying fish in gliding flight. *Journal of Experimental Biology*, 213(19):3269–3279, 2010.
- [8] Michael J Lighthill. Note on the swimming of slender fish. *Journal of Fluid Mechanics*, 9(2):305–317, 1960.
- [9] Frank E Fish, Allison Kolpas, Adam Crossett, Michael A Dudas, Keith W Moored, and Hilary Bart-Smith. Manta ray hydrodynamics: separation control mechanisms and unsteady flow characteristics. *Journal of Experimental Biology*, 219(12):1858–1871, 2016.
- [10] Koryo Miura. Method of packaging and deployment of large membranes in space. *The Institute of Space and Astronautical Science Report*, 618:1–9, 1985.
- [11] Bryan E Schubert and Dario Floreano. Variable stiffness material based on rigid low-melting-point-alloy microstructures embedded in soft poly(dimethylsiloxane)(pdms). *RSC Advances*, 3(46):24671–24679, 2013.
- [12] Michael D Bartlett, Andrew Fassler, Navid Kazem, Eric J Markvicka, and Carmel Majidi. High thermal conductivity in soft elastomers with elongated liquid metal inclusions. *Proceedings of the National Academy of Sciences*, 112(43):13206–13211, 2015.
- [13] Hyunwoo Yuk, Teng Zhang, Shaoting Lin, German A Parada, and Xuanhe Zhao. Tough bonding of hydrogels to diverse non-porous surfaces. *Nature Materials*, 15(2):190–196, 2016.
- [14] Robert Siddall and Mirko Kovač. Launching the aquatic micro-air vehicle: Bio-inspired mechanisms for water-air transition. In *2014 IEEE International Conference on Robotics and Automation (ICRA)*, pages 611–616. IEEE, 2014.
- [15] Michael J Lighthill. Large-amplitude elongated-body theory of fish locomotion. *Proceedings of the Royal Society of London. Series B. Biological Sciences*, 179(1055):125–138, 1971.
- [16] Sanjay P Sane and Michael H Dickinson. The aerodynamic effects of wing rotation and the aerodynamic basis of insect flight. *Journal of Experimental Biology*, 205(8):1087–1096, 2002.
- [17] Ludovic Righetti and Auke Jan Ijspeert. Programmable central pattern generators: an application to biped locomotion. In *Proceedings 2006 IEEE International Conference on Robotics and Automation, 2006. ICRA 2006.*, pages 1585–1590. IEEE, 2006.
- [18] Auke Jan Ijspeert. Central pattern generators for locomotion control in animals and robots: a review. *Neural Networks*, 21(4):642–653, 2008.
- [19] Joshuah K Stolaroff, Constantine Samaras, Emma R O’Neill, Alia Lubers, Anandan S Mitchell, and Daniel Ceperley. Energy use and life cycle greenhouse gas emissions of drones for commercial package delivery. *Nature Communications*, 9(1):409, 2018.